Journal of Materials Science & Technology 77 (2021) 28–37

Contents lists available at ScienceDirect

Journal of Materials Science & Technology

journal homepage: www.jmst.org

Research Article

# Liquid dynamics and glass formation of $Gd_{55}Co_{20}Al_{25}$ metallic glass with minor Si addition

Lin Xue[a,1], Liliang Shao[a,1], Qiang Luo[a], Lina Hu[b,*], Yunbo Zhao[b], Kuibo Yin[c], Mingyun Zhu[c], Litao Sun[c], Baolong Shen[a,d,**], Xiufang Bian[b]

[a] School of Materials Science and Engineering, Jiangsu Key Laboratory of Advanced Metallic Materials, Southeast University, Nanjing 211189, China
[b] School of Materials Science and Engineering, Key Laboratory for Liquid-Solid Structural Evolution and Processing of Materials (Ministry of Education), Shandong University, Jinan 250061, China
[c] SEU-FEI Nano-Pico Center, Key Laboratory of MEMS of Ministry of Education, School of Electronic Science and Engineering, Southeast University, Nanjing 210018, China
[d] Institute of Massive Amorphous Metal Science, China University of Mining and Technology, Xuzhou 221116, China

ARTICLE INFO

*Article history:*
Received 27 June 2020
Received in revised form
29 September 2020
Accepted 6 October 2020
Available online 11 November 2020

*Keywords:*
Glass-forming ability
Liquid-liquid transition
Fragile-to-strong transition
Viscosity
Relaxation

ABSTRACT

Liquid dynamics plays an essential role in glass formation. Here we observed a distinct change of liquid dynamics in $Gd_{55}Co_{20}Al_{25}$ metallic glass induced by microalloying Si element. In the equilibrium melt, minor Si (0.5 at.%) addition leads to a more fragile liquid behavior and a smaller strength of liquid-liquid transition with the transition strength ($\Delta F$) decreasing from 0.76 to 0.35. However, in the supercooled liquid, Si-doped liquid exhibits a remarkable enhanced fragile-to-strong transition (FST), and the value of FST factor $f$ increases sharply from 1.63 to 3.84, resulting in a stronger liquid behavior and more sluggish crystallization kinetics for $Gd_{55}Co_{20}Al_{24.5}Si_{0.5}$ metallic glass. Moreover, minor Si addition promotes the formation of a crystal-like structure with a size of 1–2 nm. The interactions between the crystal-like structures and other local favored clusters frustrate the further growth of crystal-like phases, thus stabilizes the amorphous structure. As a result, the glass-forming ability (GFA) was largely improved. The critical diameter of $Gd_{55}Co_{20}Al_{25}$ metallic glass increased from 2 to 7 mm with 0.5 at.% Si addition without deterioration of the magnetocaloric effect. This study provides valuable insight for understanding the distinct effect of microalloying on GFA of metallic glasses from the aspect of the evolution of the liquid.
© 2020 Published by Elsevier Ltd on behalf of The editorial office of Journal of Materials Science & Technology.

## 1. Introduction

Microalloying which has been widely used in the metallurgy and semiconductor industries is an effective method to improve the physical, chemical and mechanical properties as well as glass-forming ability (GFA) of metallic glasses (MGs) [1–4]. For instance, minor Co addition greatly improves the GFA of Ce-based bulk metallic glasses (BMGs) [2], and proper Y doping significantly enhances the GFA of Fe- and CuZr-based BMGs [5,6]. Nevertheless, the amorphous structure makes it a mystery to understand the role of microalloying in MGs. Though the experiment such as synchrotron radiation X-ray diffraction can detect statistical information of MG in one or two-dimension, it is insufficient to describe the accurate structural change induced by microalloying [7,8]. Besides, although some models and empirical criteria based on structure, thermodynamics, and kinetics have been proposed to reveal the variation of GFA with composition [9–12], the structural and dynamical origins of the effects caused by minor addition are still not clear.

As MG is formed by rapidly cooling its melt, it is expected that investigating the changes of dynamics and structure of the liquid through cooling the melt could elucidate the effect of minor addition on glass formation of MG. It is noticed that the liquid-liquid transition (LLT) in superheated liquid and the fragile-to-strong transition (FST) in supercooled liquid (SCL) have been observed in La-, Zr- and CuZr-based MG-forming liquids [13–19], both of them are reported to correlate with relaxation behavior [19,20], and the glass formations of CuZr- and Fe-based MGs have been verified beginning from LLT in their liquids [18,21]. According to

* Corresponding author.
** Corresponding author at: School of Materials Science and Engineering, Jiangsu Key Laboratory of Advanced Metallic Materials, Southeast University, Nanjing 211189, China.
*E-mail addresses:* hulina0614@sdu.edu.cn (L. Hu), blshen@seu.edu.cn (B. Shen).
[1] These authors contributed equally to this work.

https://doi.org/10.1016/j.jmst.2020.11.024
1005-0302/© 2020 Published by Elsevier Ltd on behalf of The editorial office of Journal of Materials Science & Technology.

these results, the effect of minor addition on GFA of MG is considered to be related to the liquid dynamics, i.e., LLT and FST in the superheated or supercooled liquid, from which the enhancement of GFA through microalloying may be revealed clearly.

In this work, we report the remarkable effect of minor Si addition on the glass formation and the liquid dynamics of magnetocaloric $Gd_{55}Co_{20}Al_{25}$ BMG over a wide temperature range covering the equilibrium melt, SCL and glassy solid. It was found that the diameter of $Gd_{55}Co_{20}Al_{25}$ BMG increased from 2 to 7 mm with the addition of only 0.5 at.% Si without deterioration of its magnetocaloric effect. In comparison to no obvious changes in glass transition temperature ($T_g$), crystallization temperature ($T_x$) and liquidus temperature ($T_l$), the kinetics and microstructure of $Gd_{55}Co_{20}Al_{25}$ BMG change significantly with minor Si addition. Besides, it is confirmed that the enhancement of GFA induced by minor Si addition originates from the changes of the strength of LLT and FST, which relates to the interaction and frustration between the crystal-like structures and other local favored clusters.

## 2. Materials and methods

### 2.1. Sample preparation

Ingots with nominal compositions of $Gd_{55}Co_{20}Al_{25}$ and $Gd_{55}Co_{20}Al_{24.5}Si_{0.5}$ were prepared by arc-melting a mixture of pure Gd, Co, Al, and Si with purities higher than 99.9 wt.% under a high-purity argon atmosphere. Glassy ribbons and rods were prepared by single-roller melt spinning and copper mold casting methods, respectively. In this study, ribbon samples were used for the magnetocaloric measurements to minimize the influence of demagnetization. Thin specimens for high-resolution transmission electron microscope (HRTEM) were pre-polished by the ion beam system (Gatan Inc, PIPS-M691).

### 2.2. Microstructure, thermal properties and magnetocaloric effect

Microstructures were examined by X-ray diffraction (XRD, Rigaku SmartLabXE) with $CuK_\alpha$ radiation and HRTEM observation by using an aberration-corrected TEM (Titan 80–300), respectively. Calorimetric analyses were carried out with differential scanning calorimetry (DSC, NETZSCH 404 F3). Annealing of the sample was performed by using the DSC equipment at various temperatures below $T_g$ for 60 min. The dynamical mechanical spectrums of the MGs were carried out by using a dynamical mechanical analyzer (DMA, NETZSCH 242 E) under a single cantilever bending mode with a constant heating rate of 2 K/min. Specimens with a dimension of 30 mm × 2 mm × 1 mm were prepared for the DMA measurements. Magnetocaloric properties were measured by a SQUID magnetometer (MPMS, Quantum Design). The magnetic field was applied along the length direction of ribbon. Temperature dependence of magnetization was measured upon heating from 2 to 300 K under an applied magnetic field of 0.02 T, and the isothermal magnetization was measured under a varying field from 0 to 5 T at temperatures ranging from 5 to 180 K.

### 2.3. Viscosity of the liquids

High temperature viscosity ($\eta$) was measured using a torsional oscillation viscometer [19,22]. Samples with the mass of 140 g were placed in a vessel hung by a torsional suspension wire, and a BN crucible was used to avoid reaction between the sample and container. The vessel was set to oscillate around a vertical axis, and the resulting motion was gradually damped due to frictional energy absorption and dissipation within the melt. To avoid the oxidation and get accurate viscosity data at high temperatures, all the measurements were performed under a high-purity argon atmosphere. The samples were overheated to 1723 K with a heating rate of 10 K/min and held for 30 min. Then the samples were cooled to each detected temperature and held for 20 min before the viscosity measurement to reach an equilibrium state. At each detected temperature the viscosity was measured for at least three times. The estimated uncertainty of the measurement is less than 2% under present detection conditions, and the error bar was obtained by the largest difference between the average and measured viscosity values. The interface between the sample and the crucible after the measurement was observed using a scanning electron microscope (SEM, FEI Sirion 200) with an energy disperse spectroscopy (EDS). And the viscosity data in the vicinity of $T_g$ were extrapolated by using the Mauro-Yue-Ellison-Gupta-Allan (MYEGA) equation [23]:

$$\log\eta = \log\eta_\infty + \frac{B}{T}\exp\left(\frac{C}{T}\right) \quad (1)$$

where $\eta_\infty$ is the viscosity at the high temperature limit, $B$ and $C$ are fitting parameters related to the onset of rigidity in the liquid network, with the definition of the fragility $m$ [24]:

$$m = \frac{\partial\log\eta}{\partial(T_g/T)}\Big|_{T=T_g} \quad (2)$$

For details one can refer to Ref. [23]. Fragility $m$ of the SCL was obtained by measuring the heating rate dependence of $T_g$ [25,26].

## 3. Results

### 3.1. Glass formation, magnetocaloric property and crystallization kinetics

Fig. 1(a) shows XRD patterns of the as-cast $Gd_{55}Co_{20}Al_{25}$ (Si0) and $Gd_{55}Co_{20}Al_{24.5}Si_{0.5}$ (Si0.5) BMG samples with different diameters, which display only broad diffusion humps around 33° and 57° without any sharp peaks, identifying the amorphous structure of all samples. The as-cast rods with a diameter of 7 mm exhibit smooth outer surface and good metallic luster as shown in the inset of Fig. 1(b). The amorphous structure of samples was further confirmed by DSC results shown in Fig. 1(b). As shown in the figure, all the samples exhibit a distinct glass transition followed by a supercooled liquid region and a sharp crystallization peak. It is seen that the as-cast Si0.5 rods with diameters of 2 and 7 mm show the same values of $T_g$ and $T_x$ within the experimental error, confirming the fully amorphous structure of the samples. Compared with the Si0 sample, the value of $T_g$ keeps almost unchanged, and $T_x$ increases slightly by 8 K for the Si0.5 sample. The melting and solidification curves are exhibited in the inset of Fig. 1(b). Although the two alloys possesses nearly the same melting temperature, the degree of undercooling increases from 24 to 45 K with 0.5 at.% Si addition as marked by green regions. This means the glass-forming liquid of Si0.5 alloy is more thermally stable during cooling, corresponding to better GFA [27]. Besides, the microstructure of the Si0.5 rod with a diameter of 7 mm was observed by HRTEM as shown in Fig. 1(c). The sample was selected from the central part of the rod and the maze-like pattern in the HRTEM image further confirms its fully amorphous structure. Besides, the GFA of the alloy with less or more Si addition was also studied, which increases as the Si addition increases with Si addition less than 0.5 at.% while decreases gradually with further Si addition. As Gd-based MGs are well known as promising candidates for refrigeration applications [28], the magnetocaloric effect of Si0 and Si0.5 were also measured. Fig. 1(d) shows the magnetic entropy change ($\Delta S_M$) curves as a function of temperature under a maximum magnetic field of 2 and 5 T, respectively, for Si0 and Si0.5 MGs, which are derived from Maxwell relation by integrating the corresponding isothermal magnetization curves [29]. The inset of Fig. 1(d) shows the derivative

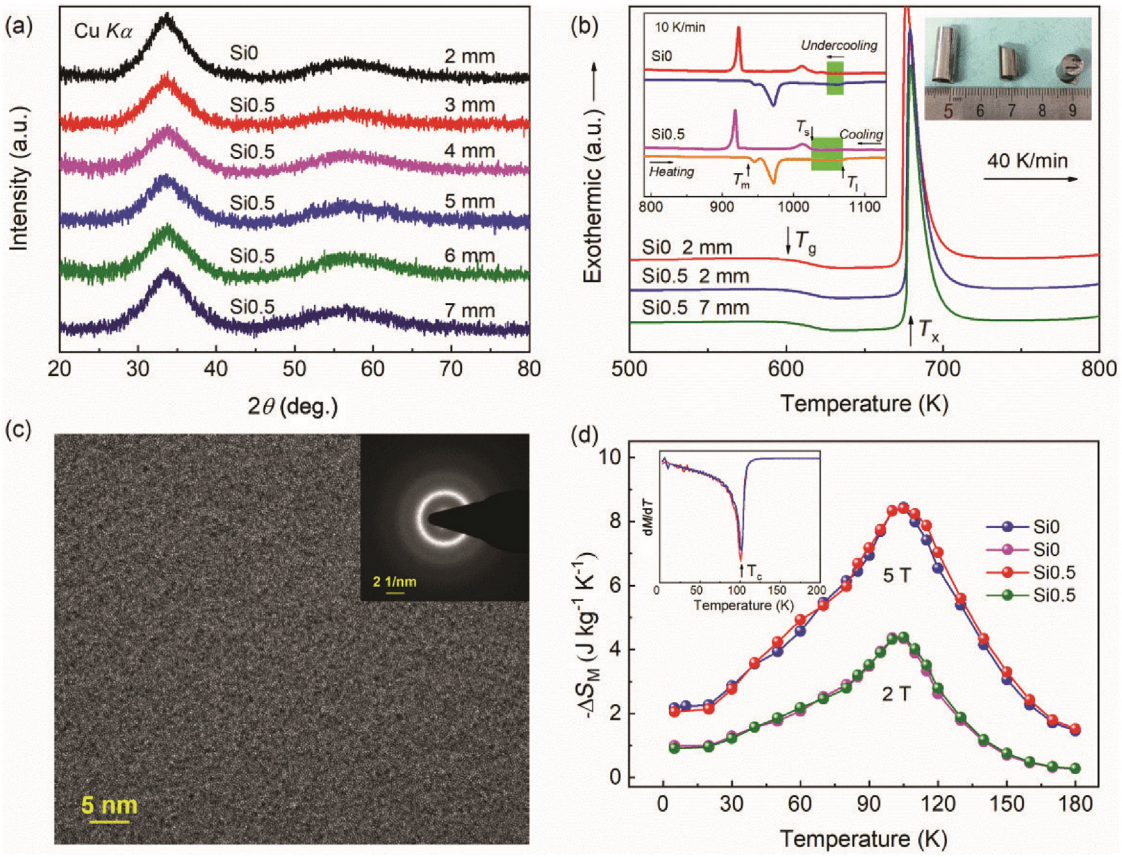


**Fig. 1.** (a) XRD patterns of the as-cast Si0 rod with a diameter of 2 mm and Si0.5 rods with diameters from 3 to 7 mm. (b) DSC traces of the Si0 glassy rod with a diameter of 2 mm and the Si0.5 glassy rods with diameters of 2 and 7 mm, the inset picture shows the photo of the Si0.5 BMG with a diameter of 7 mm. The melting and solidification curves of Si0 and Si0.5 alloys at the rate of 10 K/min are exhibited in the inset, marked with melting temperature, $T_m$, liquid temperature, $T_l$ and solidus temperature, $T_s$. (c) The HRTEM image and SAED pattern for the Si0.5 glassy rod with a diameter of 7 mm. (d) Magnetic entropy changes as a function of temperature for the Si0 and Si0.5 ribbon samples under maximum magnetic fields of 2 and 5 T, the inset shows the derivative of the temperature-dependent magnetization ($dM/dT$) curves measured under an applied field of 0.02 T.

curves of the temperature-dependent magnetization curves measured under an applied magnetic field of 0.02 T. It is seen that both MG samples possess the same value of Curie temperature ($T_C$), and no obvious difference of the $\Delta S_M$ can be observed. The maximum values of the $\Delta S_M$ under a field of 5 T are calculated to be 8.45 and 8.41 J kg$^{-1}$ K$^{-1}$ for Si0 and Si0.5 samples, respectively, demonstrating a negligible influence of microalloying Si on the magnetocaloric effect.

Although the GFA of $Gd_{55}Co_{20}Al_{25}$ BMG was largely increased with the addition of 0.5 at.% Si, the parameters such as reduced glass transition temperature ($T_{rg} = T_g/T_l$) and γ ($\gamma = T_x/(T_g+T_l)$) kept the same values. The same cases for predicting GFA by using these thermal parameters can also be found in other BMG systems [2,30]. To further understand the improvement of GFA with minor Si addition, the crystallization kinetics of Si0 and Si0.5 BMGs was investigated by isothermal annealing the samples at the temperatures of 620 and 623 K, respectively, in the SCL region as shown in Fig. 1(b). The annealing time dependence of fraction of crystallization for the two samples is shown in Fig. 2, respectively, all exhibit the usual sigmoidal type. It is seen that the incubation time and crystallization time at the temperature of 620 K are longer than those at the temperature of 623 K for both samples, indicating the slower crystallization process at lower temperatures. On the other hand, Si0.5 sample exhibits longer incubation time and crystallization time than Si0 sample at two annealing temperatures, indicating the stronger crystallization resistance of Si0.5 sample. The isothermal crystallization kinetics of amorphous alloys is normally modeled by the Johnson-Mehl-Avrami (JMA) equation:

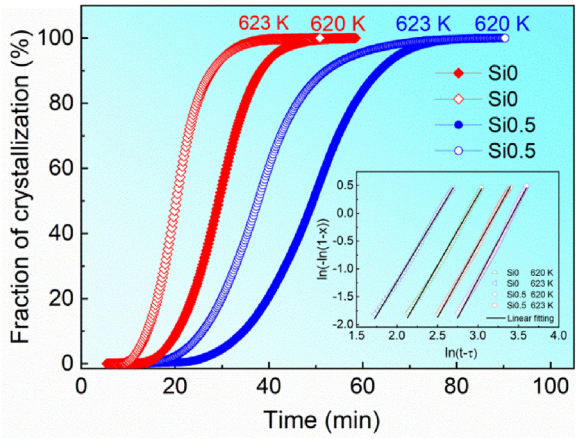


**Fig. 2.** Crystallization fractions versus annealing times for the Si0 and Si0.5 BMG samples at temperatures of 620 and 623 K. The inset shows the Avrami plots.

$x = 1 - \exp(-k(t-\tau)^n)$, where $x$ is the transformed volume fraction, $k$ is a reaction rate constant, $t$ is time, $\tau$ is the incubation time, and $n$ is the Avrami exponent [31]. When the value of $n$ is larger than 2.5, the crystallization process is considered to be dominated by diffusion-controlled growth with increasing nucleation rate. Otherwise, the crystallization process is dominated by diffusion-controlled growth with decreasing nucleation rate [31,32]. The corresponding Avrami plots are shown in the inset of Fig. 2. The

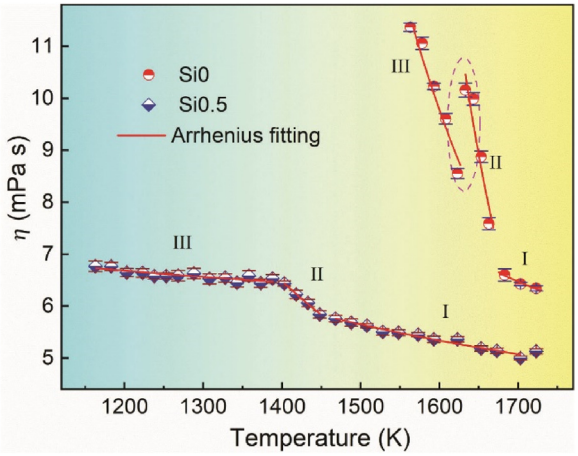


**Fig. 3.** Changes of viscosities of superheated liquids as a function of temperature for the Si0 and Si0.5 melts. Red lines are Arrhenius fitting curves. I, II, and III represent high-temperature liquid, transition region, and low-temperature liquid, respectively.

values of $n$ for Si0 samples annealed at the temperatures of 620 and 623 K are 2.53 (±0.02) and 2.42 (±0.01), respectively, indicating the crystallization process dominated by diffusion-controlled growth changes from the increase of nucleation rate to decrease of nucleation rate. For the Si0.5 samples annealed at the temperatures of 620 and 623 K, the values of $n$ are 2.75 (±0.01) and 2.61 (±0.01), respectively, implying that the crystallization process is governed by the diffusion-controlled growth with increasing nucleation rate. Further more, the values of $k$ for Si0 samples annealed at 620 and 623 K are 0.056 and 0.081, respectively, which are 0.032 and 0.040 for Si0.5 samples. The smaller values of $k$ for Si0.5 samples indicate a decrease of the nucleation and growth rates due to minor Si addition [33,34]. Generally, the sluggish kinetics corresponding to a higher viscosity of glass-forming liquid near $T_g$. To further explore the effect of minor Si addition on the GFA of the $Gd_{55}Co_{20}Al_{25}$ BMG, the dynamics of equilibrium melt and SCL, the enthalpy and slow $\beta$-relaxation of the glassy state, as well as the microstructure of Si0 and Si0.5 samples were investigated in detail.

### 3.2. Liquid-liquid transition in the superheated liquid

The relationships of viscosity and temperature for Si0 and Si0.5 melts measured from the temperatures of 600 K above $T_l$ to 1100 K are shown in Fig. 3. It needs to note that after the measurement of viscosity, the fracture surface of the ingot still exhibits metallic luster and clear boundary between the ingot and the crucible as shown in the inset of Fig. 4. The microstructure and composition examination were performed by using SEM with EDS. From the SEM image, a clear gap between the crucible and the sample can be seen, indicating that the alloy separates from the crucible. The EDS spectrums and the analyzed results in the inserted table show that the concentrations of B and N in the alloy as well as those of Gd, Co, Al and Si in the crucible can be negligible, and are consistent with the nominal compositions of each other. Besides, the mass loss after the measurements is less than 0.5 g and the increase of oxygen content is less than 0.01 wt.%, indicating that no reaction between the ingot and crucible occurred and the oxidation during the measurement was negligible. As shown in Fig. 3, different from the continuous change of viscosity observed in many melts, three stages of the viscosity change can be seen in the Si0 and Si0.5 melts, which are denoted as high-temperature liquid (I), transition region (II) and low-temperature liquid (III), indicating an existence of LLT behavior in both of the melts [19]. Besides, despite adding only 0.5 at.% Si, the difference in viscosity and temperature dependence between the Si0 and Si05 melts is large. The Si0.5 sample shows low viscosity, wide temperature range and slow change of viscosity with temperature compared to the Si0 sample, which is consistent with a larger degree of undercooling for the Si0.5 liquid as shown in the inset of Fig. 1(b). On the other hand, there is a sudden reduction of viscosity in the Si0 sample at the transition region as circled in Fig. 3, which is different from the Si0.5 sample, implying the different dynamical transition.

To quantify the dynamical behavior of the melt changing with the LLT above the temperature of $T_l$, the fragility of superheated liquid ($M$) was calculated by using the equation as below [35]:

$$M = \left|\frac{\partial\eta(T)/\partial T_l}{\partial T/\partial T_l}\right|_{T=T_l} = \left|\frac{\partial\eta_r}{\partial T_r}\right|_{T_r=1} \quad (3)$$

where $\eta_l$ is the viscosity at the temperature of $T_l$, $\eta_r$ is the ratio of $\eta$ to $\eta_l$, and $T_r$ is the ratio of $T$ to $T_l$. The $\eta$ of the low and high temperature liquids were fitted by the Arrhenius equation: $\eta = \eta_0 \exp(E/(kT))$, respectively, where $\eta_0$ is the viscosity at extremely high temperature, $E$ the activation energy, and $k$ is the Boltzmann constant [36]. As a result, fragilities of high-temperature liquid ($M_H$) and low-temperature liquid ($M_L$) were obtained, which are 2.34 and 9.88 for the Si0 melt, 0.81 and 0.60 for the Si0.5 melt, respectively, as listed in Table 1. As considering the change of $M$ during LLT, the concept of transition strength was introduced by using a parameter $\Delta F = |M_H/M_L - 1|$ [19]. The value of $\Delta F$ is 0.35 for the Si0.5 melt, which is smaller than that of 0.76 for the Si0 melt, revealing a relatively small change of the dynamical behavior and a more stable superheated liquid in the Si0.5 melt. It indicates that significant LLT in the Si0 melt is detrimental to its glass formation, which is consistent with the results of Fe-based BMGs [21].

### 3.3. Fragile-to-strong transition in the supercooled liquid

To characterize the temperature dependence of dynamical behavior of SCLs, Angell proposed the kinetic fragility [24]. The fragility is considered to correlate with many properties of the glass, such as the Boson peak, elastic behavior, interatomic repulsion softness, and relaxation [37,38]. However, glass-forming liquids may not conform to the conventional classification of SCLs, i.e., strong or fragile [17,18], and show an FST behavior which was first observed in water and later in $BeF_2$, $SiO_2$ and some others [39–41]. The existence of FST makes the correlations among fragility, glass formation, and structure evolution more complex, and raises many new open questions [41,1–44]. To understand deeply the glass formation of the Si0 and Si0.5 MGs, the liquid fragility of SCLs was investigated. The viscosities of both melts are shown in Fig. 5(a), including those of the equilibrium liquids at the temperatures above $T_l$ and the SCLs near $T_g$. The data of strong $SiO_2$, fragile OTP (orthoterphenyl) and the typical FST liquid water are also shown for comparison [17,45]. In the vicinity of $T_g$, the viscosities of the Si0 and Si0.5 melts change with Arrhenius-like behavior similar to that of $SiO_2$. On the contrary, if we extrapolate the data of viscosity from high temperature to $T_g$, relatively fragile liquid similar to OTP can be seen for the Si0.5 melt. It indicates that the metallic glass-forming liquids are relatively strong near $T_g$ while rather fragile at high temperature, showing an FST behavior similar to water. The viscosity data in melts and SCLs together with the fixed value of $10^{12}$ Pa s at $T_g$ are fitted using Eq. (1), respectively, as shown in Fig. 5(a). Thus, the fragility for the equilibrium melt above $T_l$ ($m'$) and the SCL near $T_g$ ($m$) can be determined according to Eq. (2) as listed in Table 1. Although the $m$ values of the Si0 and Si0.5 melts are 39 and 32, respectively, show a relatively strong liquid behavior near $T_g$ with a small difference, they exhibit fragile liquid dynamics above $T_l$ with a large difference in $m'$, which are 64 and 123, respectively, implying a much more fragile melt behavior for the

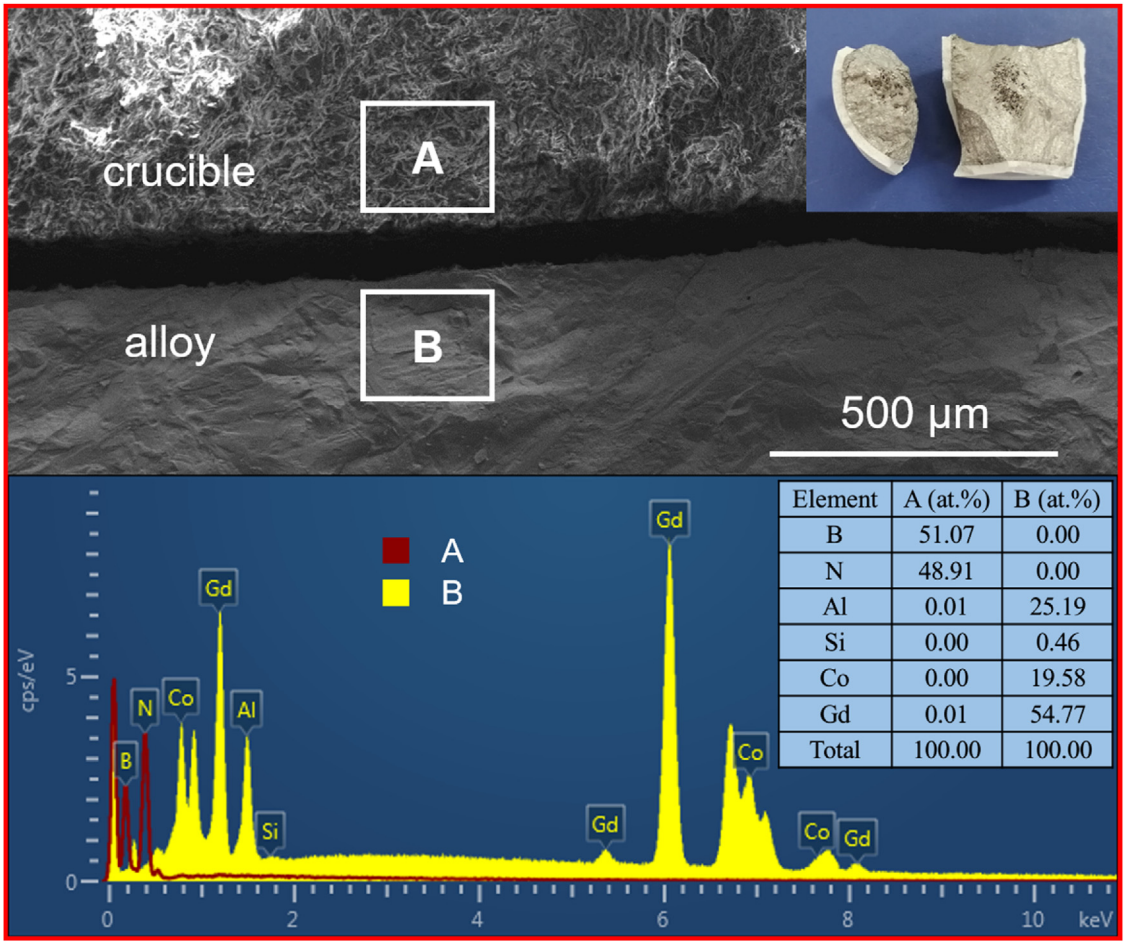


**Fig. 4.** SEM image and EDS spectrums at the vicinity of the interface between the Si0.5 alloy and crucible after the measurement of high-temperature viscosity. The inset shows the sectional view of the ingot after viscosity measurement.

**Table 1**
The data of fragilities of the high-temperature liquid ($M_H$) and low-temperature liquid ($M_L$) in superheated liquid, transition strength of LLT ($\Delta F$), fragility factors of melting liquids ($m'$) and supercooled liquids ($m$), transition magnitude ($f = m'/m$), FST temperature ($T_{fs}$), and optimized viscosity parameters using the extended MYEGA model for the Si0 and Si0.5 liquids.

| MGs | $M_H$ | $M_L$ | $\Delta F$ | $m'$ | $m$ | $f$ | $T_{fs}$ (K) | $\log\eta_\infty$ (Pa s) | $C_1$ | $C_2$ | $W_1$ | $W_2$ |
|---|---|---|---|---|---|---|---|---|---|---|---|---|
| Si0 | 2.34 | 9.88 | 0.76 | 64 | 39 | 1.63 | 960 | −2.45 | 5077.29 | 653.75 | 0.0323 | 0.000322 |
| Si0.5 | 0.81 | 0.60 | 0.35 | 123 | 32 | 3.84 | 893 | −2.25 | 13945.91 | 720.93 | 1051.97 | 0.000386 |

Si0.5 melt. The change in the fragility over the entire range of temperature is similar to the dynamic transition behavior discovered in the water by Ito *et al* [39] and other glass-forming liquids [41]. The strength of FST in liquid can be determined by a factor $f$ ($f = m'/m$), $f$ is equal to 1 means there is no FST behavior, and a larger $f$ value (>1) indicates a higher strength of FST [46]. In this study, the values of $f$ for the Si0 and Si0.5 melts are 1.63 and 3.84, respectively, which indicates a more distinct FST behavior in the Si0.5 melt during the cooling down process.

Although $f$ gives the extent of FST, it provides fewer other information of the FST. To capture more information of FST of MG liquid, a model based on the extension of the MYEGA has been used as below [17,23]:

$$\log\eta = \log\eta_\infty + \frac{1}{T\left[W_1\exp\left(-\frac{C_1}{T}\right) + W_2\exp\left(-\frac{C_2}{T}\right)\right]} \quad (4)$$

where $C_1$ and $C_2$ correspond to two constraint onset temperatures relating to two different structural mechanisms, $W_1$ and $W_2$ are normalized weighting factors, and $\log\eta_\infty$ is a pre-exponential factor shown in Table 1. Fig. 5(b) shows the fitting curves of the viscosity data using Eq. (4) with correlation ($R^2$) larger than 0.99. The fitting parameters are listed in Table 1, which can be separated into two groups dominating the fragile and strong liquids, respectively. For both Si0 and Si0.5 melts, $C_1$ is much larger than $C_2$, implying a higher activation enthalpy for dynamics in the fragile liquid. However, $W_1$ is also much larger than $W_2$, which means more transition paths and larger transition entropy for the fragile liquid. This falls in the ambit of the energy landscape framework, which elucidates a deeper (shallower) enthalpy basins but a much greater (fewer) number of escape pathways for the fragile (strong) liquid [17,42]. Thus, the change of interplay between enthalpy and entropy is critical for the occurrence of FST [39]. Such competition between enthalpy and entropy of systems has also been believed to contribute to the LLT for Pd-based MGs in SCLs [47]. The fragility diagram of the Si0.5 melt is shown in the inset of Fig. 5(b). The intersection of the fragile and the strong terms refers to the characteristic temperature of FST ($T_{fs}$), where the fragile and the strong terms have an equal contribution to liquid dynamics. As listed in Table 1, the $T_{fs}$ of the Si0 melt is 960 K, which is higher than that

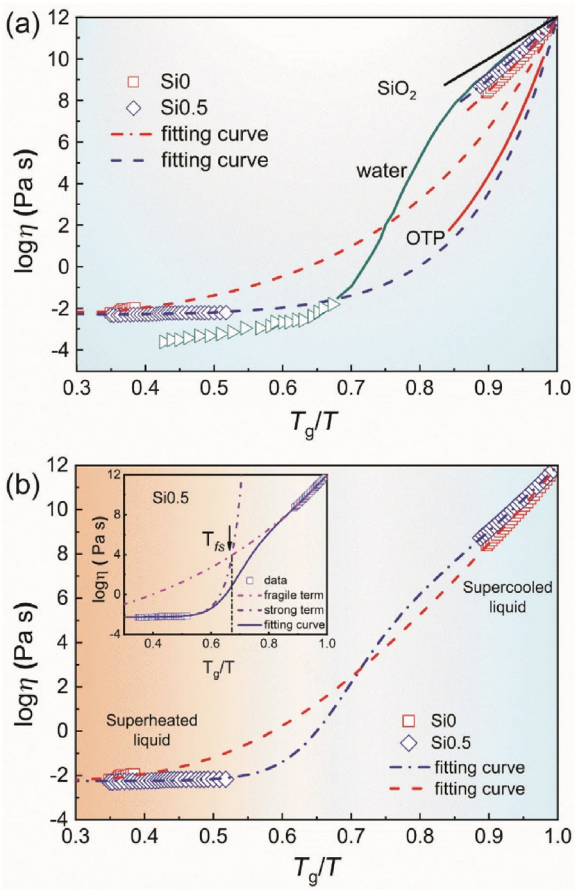


**Fig. 5.** (a) Viscosity data and fitted curves for the Si0 and Si0.5 liquids. The data of strong $SiO_2$, fragile OTP (orthoterphenyl) and the typical FST liquid water are also shown for comparison [17,45]. (b) Viscosity data and fitted curves versus $T_g/T$ for the Si0 and Si0.5 liquids, the inset shows the Angell plot for the Si0.5 liquid.

(893 K) of the Si0.5 melt. As the Si0 melt cooled approaching to $T_g$, the intervention of FST causes the viscosity to increase with a low rate compared to the Si0.5 melt. On the contrary, the Si0.5 melt exhibits a sharper FST than the Si0 melt, which is consistent with its larger value of *f*. The high strength of FST for the Si0.5 melt brings to a more stable SCL and slower atomic diffusion near $T_g$. As a result, the GFA of the Si0.5 MG was increased.

### 3.4. Relaxation of bulk metallic glasses

Relaxation of MGs not only correlates closely with the local structures of MGs but also is a good method to probe into the dynamical features of SCLs [48]. The higher the cooling rate, the more excess enthalpy can be observed in MGs. The sub-$T_g$ relaxation of MG is considered to show how the enthalpy of SCL and its structural units evolve during cooling, such as the change of the onset temperature ($T_{onset}$) at which the remnant excess enthalpy of the quenched sample begins to release [18,49]. The heat flow curves of the as-cast samples, as well as the samples annealed at different temperatures ($T_a$) with 60 min for the Si0 and Si0.5 BMGs, are shown in Fig. 6(a) and (b), respectively. For both the Si0 and Si0.5 samples, an exothermic peak followed by the endothermic glass transition peak can be seen in every curve when $T_a$ is below 527 K. Due to the increase in the stability of microstructure with low energy state, $T_{onset}$ shifts to high temperature with increasing $T_a$. It is noteworthy that the relationships between $T_{onset}$ and $T_a$ in both the Si0 and Si0.5 samples show a sudden crossover behavior around 467–482 K. Furthermore, the Si0.5 sample shows a more distinct

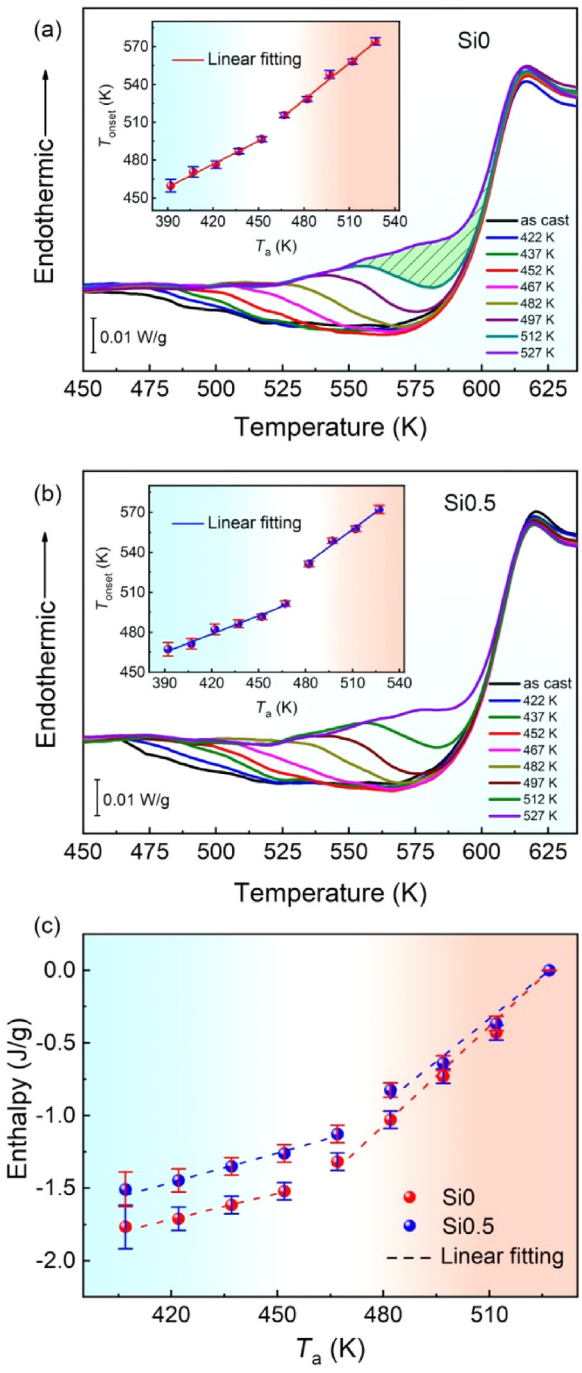


**Fig. 6.** The heat flow versus temperature for the as-cast Si0 (a) and Si0.5 (b) BMG samples after annealing at various temperatures for 60 min. The insets show the $T_{onset}$ versus annealing temperature $T_a$. (c) The excess enthalpies versus $T_a$ for the Si0 and Si0.5 BMG samples.

crossover behavior of $T_{onset}$ versus $T_a$ at a higher temperature than that of the Si0 sample as shown in Fig. 6(b). The excess enthalpies versus $T_a$ for the Si0 and Si0.5 samples calculated from Fig. 6(a) and (b) regarding the sample annealed at 527 K as a standard sample are shown in Fig. 6(c). It can be seen that the excess enthalpies for the two BMG samples release nonlinearly as the $T_a$ increases, which is consistent with that of the $T_{onset}$, indicating the discontinuous relaxation in the Si0 and Si0.5 BMGs. At the same time, the Si0.5 BMG shows the crossover behavior at a higher $T_a$ than that of Si0 BMG. The nature of the abnormal relationship between $T_{onset}$ and $T_a$ can be further investigated by DMA, which is also a useful

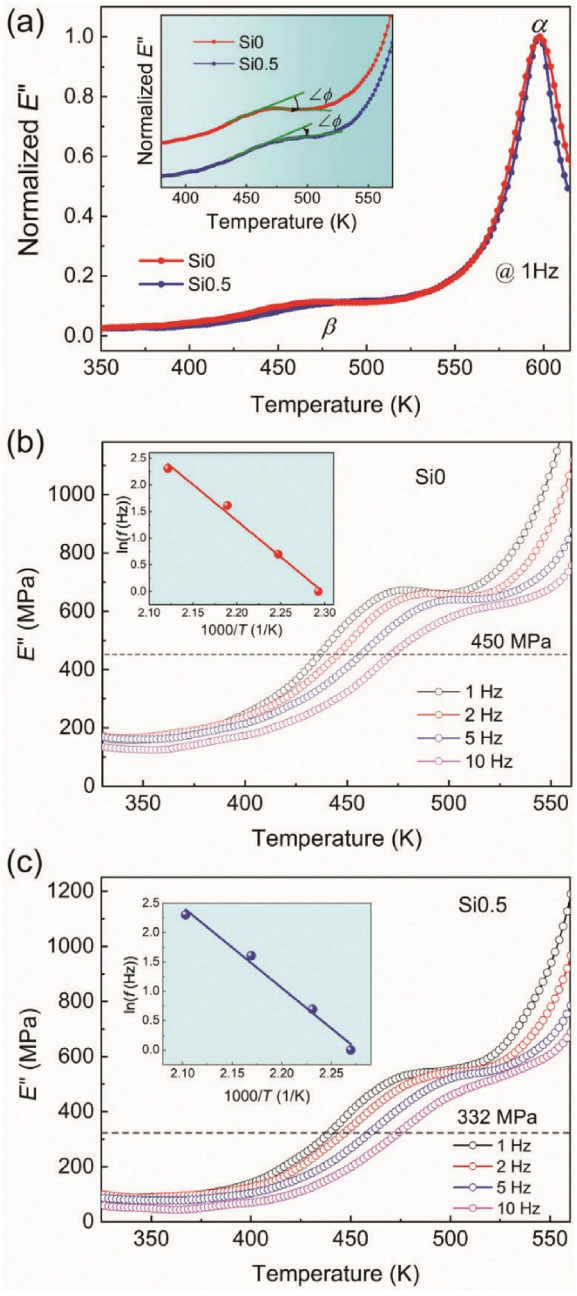


**Fig. 7.** (a) Normalized loss modulus $E^{"}$ curves at 1 Hz for the Si0 and Si0.5 BMG samples, the inset shows the angles ($\angle\phi$) exhibiting the extent of the curve line shifted from the peak of the $\beta$-relaxation for both samples. Loss modulus $E^{"}$ curves for Si0 (b) and Si0.5 (c) BMGs obtained during isothermal DMA temperature scans with various measurement frequencies from 1 to 10 Hz. The insets of (b) and (c) show Arrhenius plots to obtain $E_\beta$.

method to probe the feature of relaxation of MG through detecting the dissipation properties obtained from the loss modulus ($E^{"}$) spectrum [50].

Fig. 7(a) shows the temperature dependence of normalized $E^{"}$ for the Si0 and Si0.5 BMG samples under the frequency of 1 Hz, which exhibits a sharp $\alpha$-relaxation peak and a broad $\beta$-relaxation shoulder respectively. Fig. 7(b) and (c) shows the $\beta$-relaxation behaviors with different frequencies for the Si0 and Si0.5 samples, respectively. It is seen that the $\beta$-relaxation shoulder shifts to high temperature with increasing frequency from 1 to 10 Hz. The activation energies of $\beta$-relaxation ($E_\beta$) were calculated to be 22.6 and 22.9 $RT_g$ ($R$ is the gas constant) respectively for the Si0 and Si0.5 BMG samples, which are comparable to those of the other MGs [51,1–53]. The strength of $\beta$-relaxation can be evaluated by $T_\beta/T_\alpha$, where $T_\alpha$ and $T_\beta$ are the central temperatures of $\alpha$- and $\beta$-relaxations, and the values are 0.79 and 0.81 for the Si0 and Si0.5 samples, respectively, implying a more distinct $\beta$-relaxation in Si0 BMG [54]. The obviousness of $\beta$-relaxation of the Si0 BMG can also be confirmed by an angle ($\angle\phi$) which exhibits the extent of the curve line shifted from the peak of the $\beta$-relaxation as shown in the inset of Fig. 7(a). The values of $\angle\phi$ are determined to be 32° and 16° for the Si0 and Si0.5 samples, respectively. Accordingly, the larger $T_\beta/T_\alpha$ and smaller $\angle\phi$ for the Si0.5 BMG indicate that it is more difficult to make a distinction between the $\beta$-relaxation peak and the $\alpha$-relaxation peak, due to the structural units involved each other in the $\beta$- and $\alpha$-relaxations [55]. Note that the crossover temperatures of enthalpy relaxation in the insets of Fig. 6(a) and (b) locate in the temperature region dominated by $\beta$-relaxation, which implies that the rearrangement of the structural units responsible for $\beta$-relaxation is related to the crossover behavior of enthalpy relaxation. The higher $T_\beta$ of 484.4 K for Si0.5 BMG than that of 472.8 K for Si0 BMG reveals its higher thermal stability of the structural units for $\beta$-relaxation, and the more distinct change of $T_{onset}$ around the crossover temperature implies a higher density of structural units involved in $\beta$-relaxation for Si0.5 BMG.

## 4. Discussion

According to the results, it is clear that both Si0 and Si0.5 BMGs show sequential dynamic transitions in the melts, SCLs and glassy states. Minor Si addition caused a large change of these transitions accompanying the significant enhancement of GFA. The central temperatures of LLT observed in the superheated melts are 1650 and 1420 K for the Si0 and Si0.5 samples, respectively, as shown in Fig. 3, which are much higher than their $T_l$ of 1100–1113 K obtained by DSC measurements for both BMG samples. Consequently, the sort-range order (SRO) and medium-range order (MRO) are easy to reconstruct due to the strong thermal fluctuations. It has been found that the bond-orientational order parameter exhibits significant change around the temperature region of LLT in a La-based MG showing an LLT behavior in its melt, revealing the overall increased fraction of five-fold symmetry upon cooling through LLT [13]. In CuZrAl and CuZr melts, the molecular dynamics simulation indicates that LLT is accompanied by the increase of the rotational symmetry of local structures, the number of icosahedral-like clusters, and the enhanced connection among these clusters [14,19]. Besides, in CuZrAl metallic glass forming liquids, it was found that the FST can be attributed to the competition among the MRO clusters composed of different configurations [18,56]. The structural units at high temperature are dominantly composed of partially symmetric icosahedra in a relatively low-density state. The partially symmetric icosahedra correlate with each other to build MRO clusters upon cooling above $T_l$, while both the number and the size of the clusters are expected to increase to a critical value when cooled approaching the $T_{fs}$. To minimize the energy of the system, these clusters exhibit a tendency to dissociate or break partly down and combined into more stable ones during the FST. Further cooling below $T_{fs}$, new stable medium-range ordering clusters aggregate together into larger ones in a high-density state contributing to the strong phase [18]. Accordingly, the LLT and FST behaviors in the Si0 and Si0.5 melts in this study may result from the pronounced increase of some ordering clusters with enhanced five-fold symmetry such as icosahedral-like structures and their promoted correlation.

The effect of minor Si addition on the dynamical changes and glass formation can be discussed from the following aspects. Firstly, the radius of Si is relatively smaller than the other components

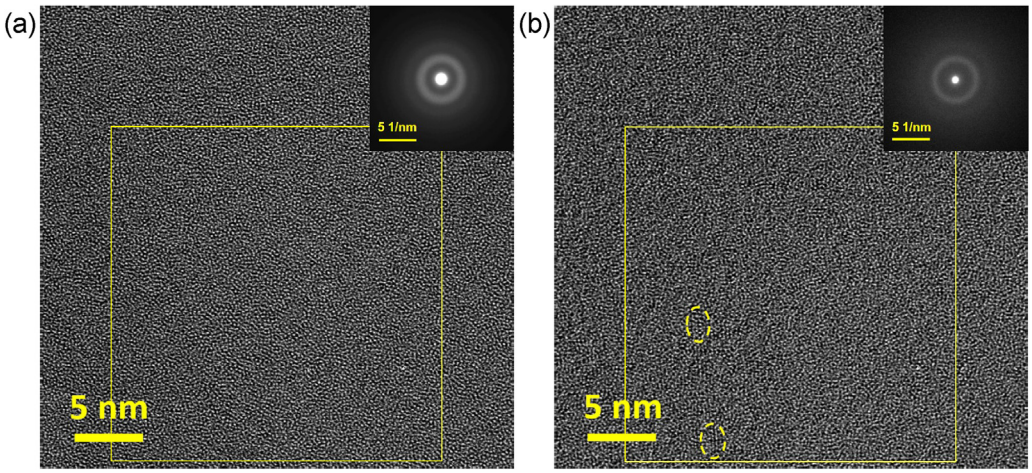


**Fig. 8.** HRTEM images and SAED patterns for the Si0 (a) and Si0.5 (b) BMG samples.

and the Si element has a large negative enthalpy of mixing with the other constituents, especially for the Gd and Co elements (-73 and −38 kJ/mol for Gd-Si and Co-Si, respectively) [57]. Therefore, the Si atoms can occupy the interstitial spaces among Gd, Co, and Al atoms, acting as linkage atoms to pull the neighboring solute-centered clusters closer to each other, during which the local symmetries of the solute-centered clusters are adjusted to enhance the packing efficiency. It was also found in a CeCuAl MG that minor Co addition (0.2 at.%) led to an obvious increase of the density and symmetry of Al-centered clusters from the $^{27}$Al NMR experiments [58]. It should be pointed out that Si can influence the packing and correlation of clusters and liquid dynamics to the utmost extent as linkage atom. From previous studies, it can be argued that minor Si addition enhances the overall fraction of five-fold symmetry, especially through increasing clusters with icosahedral-like structure, which are usually considered to be mechanically more stable and long-lived compared with others [7]. In accordance with this study, the Si0.5 BMG shows a much smaller change of viscosity above the temperature of $T_l$, much lower transition temperature and smaller strength of LLT, which means a stronger resistance for dynamic evaluation in superheated liquid owing to the increased stable solute-centered clusters. Besides, the increased packing efficiency of atomic clusters for the Si0.5 sample can be evidenced by its higher density of 7.41 g/cm$^3$ and smaller density change of 0.62 % after crystallization, which are 7.38 g/cm$^3$ and 1.08 % for Si0, respectively, in this study.

Furthermore, it was found from simulations that icosahedral clusters had a strong tendency toward self-aggregation and a remarkable correlation with other pentagon-rich clusters to form string-like networks [16,59]. For the GdAlCo(Si) liquids in this study, we argue that these favored clusters have similar aggregation features upon cooling, which plays a significant role in the FST. Minor Si addition not only increases the overall fraction of local favored clusters but also strengthens the cluster-cluster correlation. The large mixing enthalpy for Gd-Si atomic pair promotes the formation of a string-like network linked with Si atoms, which is more stable upon heating or cooling. Therefore, the dynamical mechanism of large enhancement of GFA with minor Si addition has now been elucidated from the smaller transition strength of LLT and the larger strength of FST, which is closely related to the increased fraction of local favored clusters and the enhanced correlation among theseclusters.

It has been observed that some crystal-like clusters start to form from the glass-forming melt at high temperatures to reach a lower energy state in Pd-, Fe-based MGs [60,61]. At temperatures far above $T_g$, the growth of these crystal-like clusters is limited due to the low driving force and frustration between crystal-like and icosahedral-like clusters. Under further cooling through glass transition, the crystal-like clusters tend to grow and form crystal-like superclusters [62]. In this study, except for the change of liquid dynamics, minor Si addition was also found to increase the fraction of some special crystal-like orders. Fig. 8(a) and (b) shows the HRTEM images of the Si0 and Si0.5 BMG samples with a diameter of 1 mm, which exhibit maze-like patterns demonstrating the amorphous structures. However, the Si0.5 sample shows a thinner halo ring in the SAED pattern than that of the Si0 sample, implying an increasing degree of local ordering with Si addition. As supporting evidence, some local crystal-like orders with a size of about 2 nm can be observed and were denoted by dashed circles. To quantify the areal fraction of local crystal-like order in both glasses, the square areas selected in Fig. 8(a) and (b) are divided into 144 square cells, respectively, as shown in Fig. 9(a) and (b). Each cell spans a size of 1.995 nm, close to the size of the observed crystal-like orders. Subsequently the image in each cell is transformed into its 2D auto-correlation map using auto-correlation function method which can be used to the statistical analysis of the atomic ordering in the selected region with the length scale of 1−2 nm [63,64]. The corresponding 2D auto-correlation maps are displayed in Fig. 9(a) and (b). The total areal fraction of the crystal-like regions is about 11.1 and 20.8 % for the Si0 and Si0.5 samples, respectively. This fact evidences that with minor Si addition, the local crystal-like structures formes efficiently, but the nucleation or their further growth are impeded. It seems a paradox that the crystallization process of liquids during cooling is not accelerated by such more crystal-like clusters which usually act as crystallization nuclei. This situation should be related to the increased fraction of SRO clusters with enhanced five-fold local symmetry. These favored SRO clusters may pin the boundary of the crystal-like clusters and thus impede their growth [62]. Besides, the Si atoms should mainly locate at the interfaces between crystal-like structures and other clusters, the strong Gd-Si bonds make these interfaces rather stable. Besides, the enhanced packing density with Si addition provides less space for rearrangements of atoms, making the crystal-like clusters more difficult to grow. Due to the frustrated growth of the crystal-like order, the enhanced overall structural ordering reduces the free energy of the liquid, and thus decreases the free-energy difference between the liquid and crystalline phase ($\Delta G^{l-c}$). According to the relation: $\Delta G^* = 16\pi\gamma_{l-c}^3/3(\Delta G^{l-c})^2$, where $\Delta G^*$ is the free energy barrier and $\gamma_{l-c}$ is the interface tension between the crystal and liquid [65], $\Delta G^*$ increases with Si addition for a given $\gamma_{l-c}$, indicating the enhancement of crystallization resistance. Therefore, the frustration and interaction between crystal-like clusters and other local

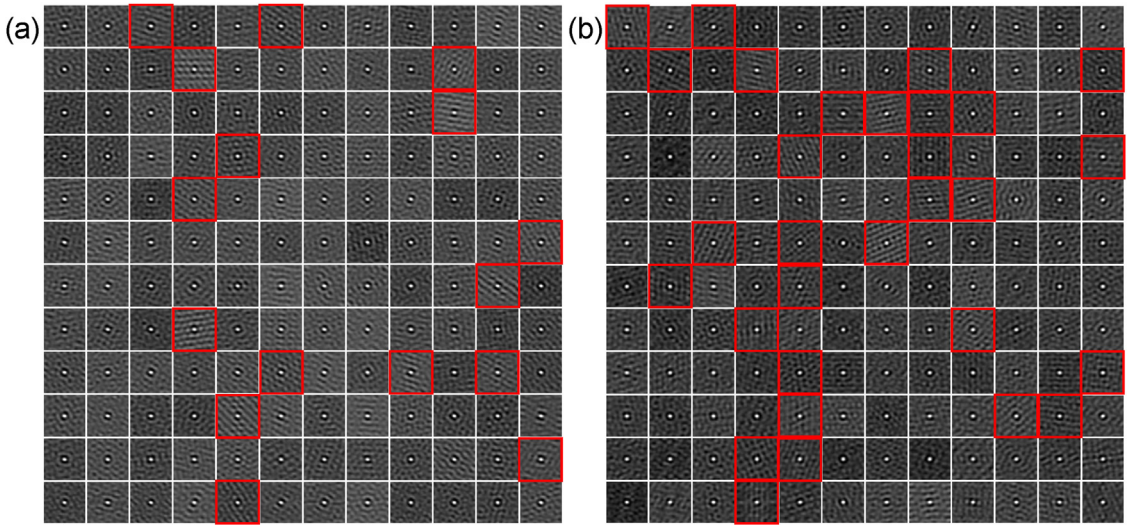


**Fig. 9.** The segmentation of the selected squares in Fig. 8(a) and (b) for auto-correlation analysis of the Si0 (a) and Si0.5 (b) BMG samples, respectively. The dimension of each segment or cell is 1.995 nm × 1.995 nm.

favored clusters, explicate structurally the improvement of GFA by minor Si addition.

## 5. Conclusion

In conclusion, the GFA of $Gd_{55}Co_{20}Al_{25}$ BMG is considerably enhanced with 0.5 at.% Si addition with the diameter increasing from 2 to 7 mm without deterioration of its magnetocaloric effect. The glass formation is comprehended on a systematic and in-depth level by exploring the whole dynamic slowdown from equilibrium melts, SCLs, to glassy states. With minor Si addition, the central temperature of LLT decreases from 1650 to 1420 K and the FST temperature decreases from 960 to 892 K with the value of $f$ increasing from 1.63 to 3.84. LLT and FST behaviors are found to be crucial for understanding the improvement of GFA from the viewpoint of liquid dynamics. The Si0.5 BMG reverses its apparent adverse state through LLT and FST, which exhibits a smaller viscosity and a lager fragility parameter $m'$ than those of the Si0 BMG, and finally shows a larger viscosity and slightly stronger liquid behavior around $T_g$, leading to increase GFA. It is rather striking that all the LLT, FST, glass formation and glassy kinetics in the vicinity of $T_g$ show distinct change with minor Si addition. The Si element serves as linkage atoms, changing significantly the correlation and interaction of neighboring clusters and promoting the formation of crystal-like structures with a size of 1–2 nm and other stable clusters. The aggregation and correlation between these favored clusters could relate to the formation of the string-like network and play a significant role in the LLT, FST, and glassy dynamics. This work not only uncovers the effect of minor addition on the dynamic slowdown and improvement of GFA but also give route to study the liquid-solid correlations of metallic melts.

## Author contributions

B.L. Shen conceived this study. L Xue and L.L. Shao designed and performed most of the experiments and data analyses with support from L.N. Hu, X.F. Bian, K.B. Yin and L.T. Sun. L Xue and Y.B. Zhao measured the viscosity of the melts. L.L. Shao and M.Y. Zhu carried out the HRTEM observations. L. Xue and L.L. Shao wrote the manuscript with support from Q. Luo, L.N. Hu and B.L. Shen. All authors contributed to the general discussion.

## Acknowledgements

This work was financially supported by the National Natural Science Foundation of China (Nos. 51631003, 51571131, 51971061 and 51471050) and the National Key Research Program of China (No. 2016YFB0300500).

## References

[1] W.H. Wang, Prog. Mater. Sci. 52 (2007) 540–596.
[2] B. Zhang, R.J. Wang, D.Q. Zhao, M.X. Pan, W.H. Wang,Phys. Rev. B 73 (2006), 092201.
[3] P.B. Chen, T. Liu, F.Y. Kong, A.D. Wang, C.Y. Yu, G. Wang, C.T. Chang, X.M. Wang, J. Mater. Sci. Technol. 34 (2018) 793–798.
[4] Q. Li, B.L. Shen, IEEE Trans. Magn. 57 (2011) 2490–2493.
[5] Z.P. Lu, C.T. Liu, W.D. Porter, Appl. Phys. Lett. 83 (2003) 2581.
[6] D.H. Xu, G. Duan, W.L. Johnson,Phys. Rev. Lett. 92 (2004), 245504.
[7] S.G. Hao, C.Z. Wang, M.J. Kramer, K.M. Ho,J. Appl. Phys. 107 (2010), 053511.
[8] S. Mukherjee, J. Schroers, Z. Zhou, W.L. Johnson, W.K. Rhim, Acta Mater. 52 (2004) 3689–3695.
[9] Z.P. Lu, C.T. Liu,Phys. Rev. Lett. 91 (2003), 115505.
[10] H. Ma, L.L. Shi, J. Xu, Y. Li, E. Ma,Appl. Phys. Lett. 87 (2005), 181915.
[11] Y.Q. Cheng, E. Ma, Prog. Mater. Sci. 56 (2011) 379–473.
[12] L.L. Shao, L. Xue, Q. Luo, Q.Q. Wang, B.L. Shen,Materialia 7 (2019), 100419.
[13] W. Xu, M.T. Sandor, Y. Yu, H.B. Ke, H.P. Zhang, M.Z. Li, W.H. Wang, L. Liu, Y. Wu, Nat. Commun. 6 (2015) 7696.
[14] C. Zhou, L.N. Hu, Q.J. Sun, J. Qin, X.F. Bian, Y.Z. Yue,Appl. Phys. Lett. 103 (2013), 171904.
[15] S. Wei, F. Yang, J. Bednarcik, I. Kaban, O. Shuleshova, A. Meyer, R. Busch, Nat. Commun. 4 (2013) 2083.
[16] K.N. Lad, N. Jakse, A. Pasturel,J. Chem. Phys. 136 (2012), 104509.
[17] C.Z. Zhang, L.N. Hu, Y.Z. Yue, J.C. Mauro,J. Chem. Phys. 133 (2010), 014508.
[18] C. Zhou, L.N. Hu, Q.J. Sun, H. Zheng, C.Z. Zhang, Y.Z. Yue,J. Chem. Phys. 142 (2015), 064508.
[19] X. Zhao, C.Z. Wang, H.J. Zheng, Z.A. Tian, L.N. Hu, Phys. Chem. Chem. Phys. 19 (2017) 15962–15972.
[20] X.N. Yang, C. Zhou, Q.J. Sun, L.N. Hu, J.C. Mauro, C.Z. Wang, Y.Z. Yue, J. Phys. Chem. B 118 (2014) 10258–10265.
[21] H.J. Zheng, L.N. Hu, X. Zhao, C.Z. Wang, Q.J. Sun, T. Wang, X.D. Hui, Y.Z. Yue, X.F. Bian, J. Non-Cryst. Solids 471 (2017) 120–127.
[22] R. Roscoe, Proc. Phys. Soc. London 72 (1958) 576–584.
[23] J.C. Mauro, Y.Z. Yue, A.J. Ellison, P.K. Gupta, D.C. Allan, Proc. Natl. Acad. Sci. U.S.A. 106 (2009) 19780–19784.
[24] C.A. Angell, Science 267 (1995) 1924–1935.
[25] R. Brüning, K. Samwer, Phys. Rev. B 46 (1992) 11318.
[26] R. Böhmer, K.L. Ngai, C.A. Angell, D.J. Plazek, J. Chem. Phys. 99 (1993) 4201.
[27] M. Yang, X.J. Liu, Y. Wu, H. Wang, X.Z. Wang, Z.P. Lu, Mater. Res. Lett. 6 (2018) 495–500.
[28] V. Franco, J.S. Blázquez, J.J. Ipus, J.Y. Law, L.M. Moreno-Ramírez, A. Conde, Prog. Mater. Sci. 93 (2018) 112–232.
[29] K.A. Gschneidner, V.K. Pecharsky, Annu. Rev. Mater. Sci. 30 (2000) 387–429.
[30] W.M. Yang, H.S. Liu, C.C. Dun, J. Li, Y. Zhao, B.L. Shen, J. Non-Cryst. Solids 361 (2013) 82–85.

[31] J. Malek, Thermochim. Acta 267 (1995) 61–73.
[32] J.W. Christian, The Theory of Transformations in Metals and Alloys, third ed., Pergamon, New York, 2002.
[33] T. Pradell, D. Crespo, N. Clavaguera, M.T. Clavaguera-Mora, J. Phys. Condens. Matter 10 (1998) 3833–3844.
[34] M.T. Clavaguera-Mora, N. Clavaguera, D. Crespo, T. Pradell, Prog. Mater. Sci. 47 (2002) 559–619.
[35] X.F. Bian, B.A. Sun, L.N. Hu, Y.B. Jia, Phys. Lett. A 335 (2005) 61–67.
[36] S. Nishimura, S. Matsumoto, K. Terashima, J. Cryst. Growth 237 (2002) 1667–1670.
[37] S.N. Yannopoulos, G.P. Johari, Nature 442 (2006) E7–E8.
[38] W.H. Wang, Prog. Mater. Sci. 57 (2012) 487–656.
[39] K. Ito, C.T. Moynihan, C.A. Angell, Nature 398 (1999) 492–495.
[40] M. Hemmati, C.T. Moynihan, C.A. Angell, J. Chem. Phys. 115 (2001) 6663–6671.
[41] I. Saika-Voivod, P.H. Poole, F. Sciortino, Nature 412 (2001) 514–517.
[42] H. Tanaka, J. Phys. Condens. Matter 15 (2003) L703–L711.
[43] J. Hedstrom, J. Swenson, R. Bergman, H. Jansson, S. Kittaka, Eur. Phys. J.: Special Topics 141 (2007) 53–56.
[44] S.H. Chong, S.H. Chen, F. Mallamace,J. Phys. Condens. Matter 21 (2009), 504101.
[45] K.L. Ngai, S. Capaccioli,Phys. Rev. E 69 (2004), 031501.
[46] Q.J. Sun, C. Zhou, Y.Z. Yue, L.N. Hu, J. Phys. Chem. Lett. 5 (2014) 1170–1174.
[47] S. Lan, Y. Ren, X.Y. Wei, B. Wang, E.P. Gilbert, T. Shibayama, S. Watanabe, M. Ohnuma, X.L. Wang, Nat. Commun. 8 (2017) 14679.
[48] J.C. Qiao, Q. Wang, J.M. Pelletier, H. Kato, R. Casalini, D. Crespo, E. Pineda, Y. Yao, Y. Yang, Prog. Mater. Sci. 104 (2019) 250–329.
[49] J.C. Qiao, J.M. Pelletier, J. Mater. Sci. Technol. 30 (2014) 523–545.
[50] M. Frey, R. Busch, W. Possart, I. Gallino, Acta Mater. 155 (2018) 117–127.
[51] H.B. Yu, W.H. Wang, H.Y. Bai, Y. Wu, M.W. Chen,Phys. Rev. B 81 (2010), 220201.
[52] J.C. Qiao, Y.H. Chen, R. Casalini, J.M. Pelletier, Y. Yao, J. Mater. Sci. Technol. 35 (2019) 982–986.
[53] H.B. Yu, W.H. Wang, K. Samwer, Mater. Today 16 (2013) 183–191.
[54] P. Luo, Z. Lu, Z.G. Zhu, Y.Z. Li, H.Y. Bai, W.H. Wang,Appl. Phys. Lett. 106 (2015), 031907.
[55] H.B. Yu, Z. Wang, W.H. Wang, H.Y. Bai, J. Non-Cryst. Solids 358 (2012) 869–871.
[56] L.N. Hu, C. Zhou, C.Z. Zhang, Y.Z. Yue,J. Chem. Phys. 138 (2013), 174508.
[57] A. Takeuchi, A. Inoue, Mater. Trans. 46 (2005) 2817–2829.
[58] X.K. Xi, L.L. Li, B. Zhang, W.H. Wang, Y. Wu,Phys. Rev. Lett. 99 (2007), 095501.
[59] M.Z. Li, C.Z. Wang, S.G. Hao, M.J. Kramer, K.M. Ho,Phys. Rev. B 80 (2009), 184201.
[60] T. Ichitsubo, E. Matsubara, T. Yamamoto, H.S. Chen, N. Nishiyama, J. Saida, K. Anazawa,Phys. Rev. Lett. 95 (2005), 245501.
[61] A.S. Nouri, Y. Liu, J.J. Lewandowski, Metall. Mater. Trans. A 40 (2009) 1314–1323.
[62] Q. Wang, C.T. Liu, Y. Yang, J.B. Liu, Y.D. Dong, J. Lu, Sci. Rep. 4 (2014) 4648.
[63] G.Y. Fan, J.M. Cowley, Ultramicroscopy 17 (1985) 345–355.
[64] X.J. Liu, G.L. Chen, H.Y. Hou, X. Hui, K.F. Yao, Z.P. Lu, C.T. Liu, Acta Mater. 56 (2008) 2760–2769.
[65] D. Turnbull, Contemp. Phys. 10 (1969) 473–488.